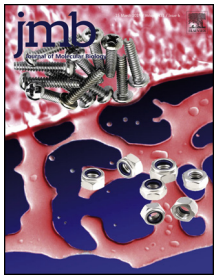

Multiple Mechanisms Are Involved in Repression of Filamentous Phage SW1 Transcription by the DNA-Binding Protein FpsR

Huahua Jian [1,2,3,†], Guanpeng Xu [1,†], Shunzhang Liu [1,†], Yali Hao [1], Canxing Meng [1], Jianrong Xu [4], Yue Zhang [1], Xipeng Liu [1] and Xiang Xiao [1,2,3]

*1 - **State Key Laboratory of Microbial Metabolism,** School of Life Sciences and Biotechnology, Shanghai Jiao Tong University, Shanghai 200240, PR China*
*2 - **State Key Laboratory of Ocean Engineering,** School of Naval Architecture, Ocean and Civil Engineering, Shanghai Jiao Tong University, Shanghai 200240, PR China*
*3 - **Laboratory for Marine Biology and Biotechnology,** Qingdao National Laboratory for Marine Science and Technology, Qingdao 266237, PR China*
*4 - **Department of Pharmacology and Chemical Biology,** Institute of Medical Sciences, School of Medicine, Shanghai Jiao Tong University, Shanghai 200025, PR China*

***Correspondence to Xiang Xiao:** Shanghai Jiao Tong University, Mulan Building, Room 325, Shanghai 200240, PR China.*
zjxiao2018@sjtu.edu.cn
https://doi.org/10.1016/j.jmb.2019.01.040
Edited by John Johnson

Abstract

SW1 is the first filamentous phage isolated from a deep-sea environment. Nevertheless, the mechanism by which the SW1 genetic switch is controlled is largely unknown. In this study, the function of the phage-encoded FpsR protein was characterized by molecular biological and biochemical analyses. The deletion of *fpsR* increased the copy number of SW1 ssDNA and mRNA, indicating that FpsR functions as a repressor. In addition, transcription from the *fpsR* promoter was shown to be increased in an *fpsR* deletion mutant, suggesting self-repression by FpsR. Purified FpsR bound to four adjacent operator sites (*O1–O4*) embedded within the *fpsA* promoter and the *fpsA–fpsR* intergenic region. A surface plasmon resonance experiment showed that FpsR can bind to the *O1–O4* operators separately and with different binding affinity, and the dissociation constants of FpsR with *O2* and *O3* were found to be lower at 4 °C than at 20 °C. A gel permeation chromatography assay revealed that FpsR oligomerized to form tetramers. Point mutation analysis indicated that the C-terminal domain influenced the binding affinity and regulatory function of FpsR. Collectively, these data support a model in which FpsR actively regulates phage production by interacting with the corresponding operators, thus playing a crucial role in the SW1 genetic switch.

Introduction

Viruses are believed to be the most abundant biological agents in the ocean [1–4], and they play an important role in microbial metabolism, prokaryotic mortality, and nutrient recycling in deep-sea ecosystems, thus significantly influencing the geochemical cycles of our planet [5–8]. However, the induction mechanism of the benthic viruses is largely unknown. Previously, a filamentous phage, SW1, was identified and characterized in the deep-sea bacterium *Shewanella piezotolerans* WP3 (hereafter referred to as WP3), which was isolated from sediment in the West Pacific at a water depth of 1914 m [9–11]. Interestingly, the generation of phage particles was significantly increased at 4 °C, and the transcription of phage SW1 genes was higher at 4 °C than at 25 °C or 15 °C, indicating that SW1 is a cold-active bacteriophage [9]. There are three forms of phage SW1 DNA in the WP3 host cells: integrated prophage, replicative double-stranded DNA (RF DNA), and single-stranded DNA (ssDNA), which will be incorporated into the phage particles [12]. The copy number of SW1 RF DNA was found to be temperature and growth phase dependent, whereas the ssDNA of SW1 was only produced at 4 °C [12]. The SW1 genome was demonstrated to include two operons and exceptionally long 5′ untranslated regions (UTRs) that regulate the stability of the SW1

RNA transcript, thus revealing a role for posttranscriptional regulation in the cold induction of SW1 [13].

Temperate bacteriophages commonly encode transcriptional repressors that control the genetic switch and determine the selection of the lysogenic or lytic pathway [14]. The CI repressor that regulates the bacteriophage lytic-lysogeny switch has been most extensively studied in phage λ and its close relatives [15–22]. CI repressors from these phages usually consist of an N-terminal helix-turn-helix domain and a C-terminal oligomerization domain connected by a linker [16,23]. The structure of the phage λ repressor CI has been determined, and it has a special architecture that facilitates pairwise cooperative binding to two sets of three operator sites [16]. Furthermore, the functional modules of the CI repressor in lactococcal phage TP901-1 and staphylococcal phage Φ11 have also been investigated in detail [15,17–19,21,24–27].

Filamentous phages, which contain a circular ssDNA genome, have been identified in various gram-negative bacteria that inhabit diverse environments [28–30]. The most prominent characteristic of this type of phage is the absence of lysis of the host bacteria when the phage enters the "lytic" state and phage particles are released [29]. Several filamentous phages have been shown to carry transcriptional repressors [30]. The CTXΦ repressor RstR was demonstrated to form tetramers when bound to the three operator sites that are located in the *rstA* promoter region [31]. RstR represses the transcription originating from the *rstA* promoter, thereby controlling the expression of all the CTXΦ genes required for phage production [31,32]. In addition, the function of repressors in the ΦRSM and cf1 phages has also been investigated [33–35].

As the sole gene annotated as a transcriptional regulator in the SW1 genome, the *fpsR* gene is oriented in the reverse direction from the other eight ORFs of SW1 [9,13]. The transcription of *fpsR* was demonstrated to be cold inducible and to reach its highest level in the exponential phase [12]. A previous study indicated that *fpsR*-encoded FpsR was able to bind to the promoter region of *fpsA*, suggesting that FpsR may regulate gene transcription in SW1 by direct binding [13]. However, FpsR cannot bind to the promoter of the *fpsR* gene, thus evoking the questions of whether the self-repression of *fpsR* exists and how it is regulated [13]. In this study, we present evidence to support a regulatory model that explains how FpsR is self-repressed and how it regulates the SW1 genetic switch.

Results

Construction of the *fpsR* deletion mutant

To investigate the function of *fpsR* in the gene expression of SW1, we have tried to knock out the *fpsR* gene in WP3 wild-type strain, which harbors integrated prophage and SW1 RF DNA (Fig. 1a). However, these attempts always ended in failure (data not shown). We supposed that the RF DNA of SW1 could compensate the deletion in the prophage, thus leading to the unsuccessful deletion of *fpsR* gene in WP3 wild-type strain. In order to solve this problem, an *fpsR* deletion vector, pSW2Δ*fpsR*, was constructed based on the *Escherichia coli–Shewanella* shuttle vector pSW2 [36], which contains the complete sequence of *fpsR–fpsD* (Fig. 1b). The pSW2 vector and its derived vector were then introduced into the phage-free WP3 strain WP3ΔSW1 to generate the WP3ΔSW1–pSW2 and WP3ΔSW1–pSW2Δ*fpsR* strains, respectively (Fig. 1b). Notably, the SW1 regulatory region that contains promoters of *fpsA* and *fpsR* was completely retained in pSW2 (Fig. 1c). Therefore, the function of FpsR in the gene expression of SW1 was investigated with the WP3ΔSW1/pSW2 system in the following study.

FpsR negatively regulates DNA replication, gene transcription and phage production in SW1

Initially, the putative impact of FpsR on the growth of WP3 was investigated. No growth deficiency of WP3ΔSW1–pSW2Δ*fpsR* was observed when the strain was cultivated at 20 °C (the optimal growth temperature of WP3) (Fig. 2a). These data are consistent with those from our previous study, in which SW1 was not observed to influence the growth of WP3 at either temperature (20 °C and 4 °C) [37]. Total DNA was extracted, and the copy number of the RF DNA and ssDNA of pSW2 and pSW2Δ*fpsR* was quantified. The data showed that the copy number of the RF DNA of these two vectors was similar at both growth phases, except that it slightly decreased in pSW2Δ*fpsR* at the late exponential phase (Fig. 2b). Notably, no pSW2 ssDNA was produced, whereas ssDNA was substantially produced after *fpsR* was deleted, indicating that the genetic switch of SW1 was turned on under these circumstances (Fig. 2c).

Subsequently, the influence of FpsR on gene transcription in SW1 was investigated. Two genes, *fpsA* and *fpsB*, which encode a replication protein (FpsA) and an ssDNA binding protein (FpsB) and are located in the same operon, were chosen as representatives. As the copy number of RF DNA (the transcription template of SW1 genes) is various in different vectors and growth phases (Fig. 2b), it is uncertain whether the observed change in mRNA quantity is the effect of a change in DNA copy number or whether the transcription level per gene is also affected. Therefore, the relative transcription level (RTL) of *fpsA* and *fpsB* was calculated by calibrating the number of transcripts per RF DNA. In general, the RTLs of *fpsA* and *fpsB* were significantly higher, approximately 4- and 5-fold, respectively,

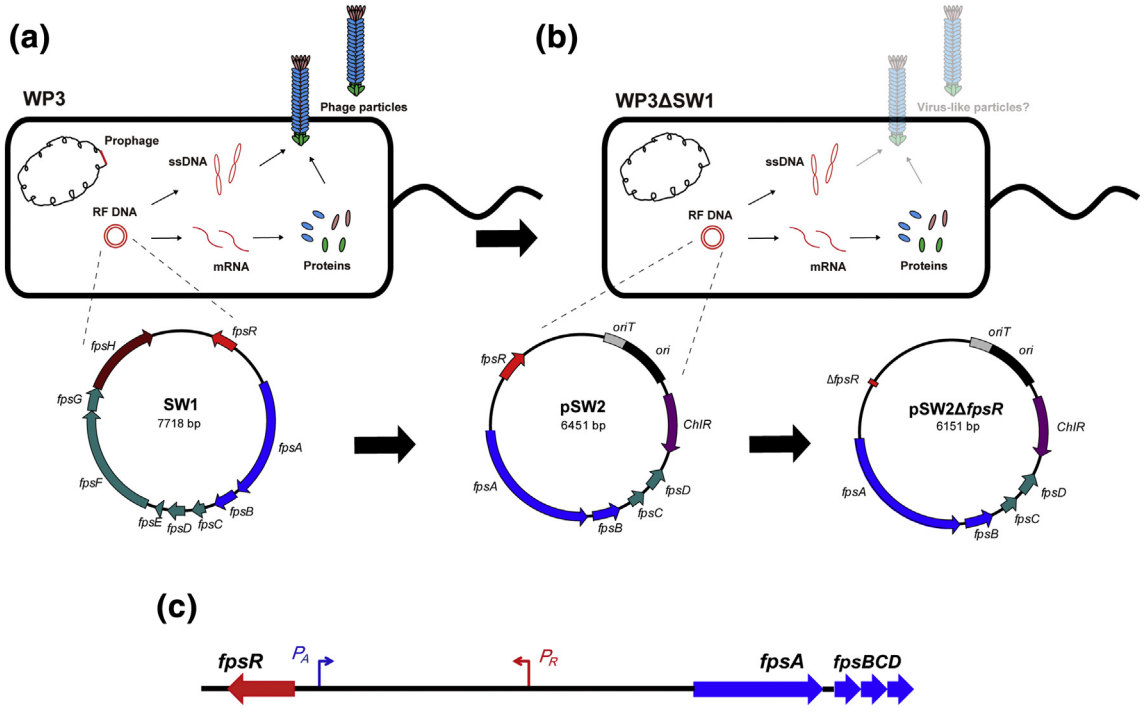

Fig. 1. Investigation of the function of FpsR with the WP3ΔSW1/pSW2 system. (a) The lysogenic WP3 cell contains multiple forms of phage SW1 DNA: The chromosomally integrated prophage, the double-strand RF DNA and the circular ssDNA. RF DNA serves as a template for ssDNA and mRNA synthesis. The virion of phage is composed of ssDNA and coat proteins. (b) Construction of the *fpsR* deletion mutant based on the pSW2 vector. Previously, the phage-free WP3 strain WP3ΔSW1 and the shuttle vector pSW2 were constructed, respectively [36,37]. The pSW2 components include the majority of SW1 genome (*fpsABCDR* genes and the regulatory region). A detailed methodology for the construction of pSW2Δ*fpsR* can be found in the Materials and Methods section. (c) Schematic representation of the regulatory region of filamentous phage SW1. Two key promoters (P_A and P_R) are represented as arrows. Notably, the transcription directions of *fpsA* and *fpsR* are arranged in an uncommon opposite direction.

in pSW2Δ*fpsR* than in pSW2 during the late exponential phase (Fig. 2d and e), indicating that FpsR negatively modulated phage SW1 transcription to some extent.

Although we were not sure that pSW2 could produce intact virus-like particles (VLPs) because pSW2 lacks four structural genes (*fpsE–H*) found in SW1, we tried to examine pSW2-produced VLPs by fluorescence microcopy. The results showed that pSW2 can still produce VLPs and that the deletion of *fpsR* significantly increased the number of VLPs (Fig. S1). These data are in accordance with those for the quantification of ssDNA and support the conclusion that FpsR is a crucial repressor that controls SW1 production.

To clarify the FpsR-mediated regulation at low temperature, the WP3ΔSW1–pSW2 and WP3ΔSW1–pSW2Δ*fpsR* strains were cultivated at 4 °C, which is the induction temperature of phage SW1 [9,12]. No growth deficiency of WP3ΔSW1–pSW2Δ*fpsR* was observed compared with WP3ΔSW1–pSW2 (Fig. S2a). As expected, a significant amount of pSW2 ssDNA was generated at 4 °C. Interestingly, the copy number of pSW2Δ*fpsR* ssDNA was 3-fold higher than that of pSW2 ssDNA (Fig. S2c), and similar change of RTL of *fpsA* and *fpsB* was detected at 4 °C (Fig. S2d and S2e), suggesting that FpsR is still partially functional as a repressor at low temperature, despite the fact that phage SW1 ssDNA production is active.

fpsR is self-repressed by FpsR at the transcription level

In a previous study, *fpsR* and its downstream 3′ UTR were shown to reside in a single operon controlled by the *fpsR* promoter [13]. To test whether FpsR can represses its own gene expression, a primer pair located in the 3′UTR of *fpsR* was used to quantify the transcription from P_R (Fig. 3a). As shown in Fig. 3b, the RTL of the *fpsR* 3′UTR of was significantly increased in the *fpsR* deletion mutant pSW2Δ*fpsR* compared with that in pSW2, indicating that the transcription of the *fpsR* operon is self-repressed by FpsR. Similar results were observed at 4 °C (Fig. S2f), suggesting that the self-repression of FpsR is independent of temperature.

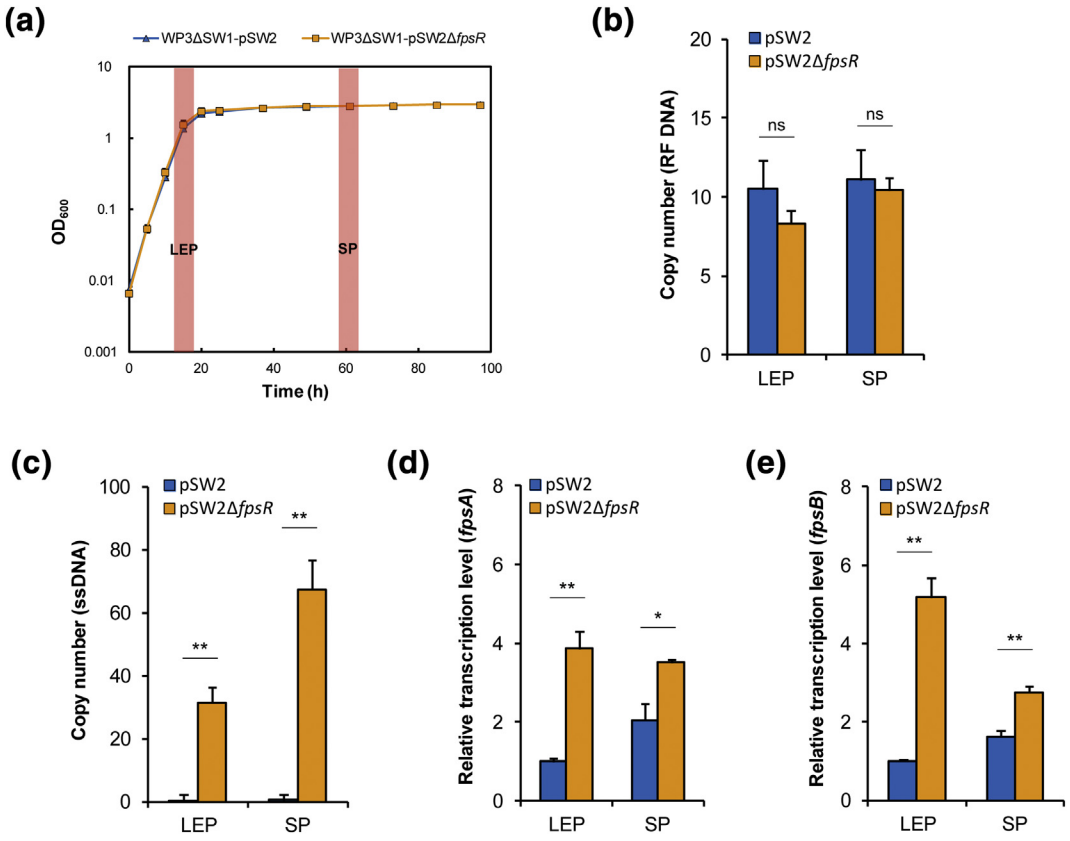

Fig. 2. The influence of *fpsR* deletion on the DNA replication and gene transcription of SW1. (a) Growth curves for WP3ΔSW1–pSW2 and WP3ΔSW1–pSW2Δ*fpsR*. The assay was performed in 2216E medium at 20 °C, and the different growth phases are indicated with gray bars. LEP: late exponential phase; SP: stationary phase. (b and c) Copy number of pSW2Δ*fpsR* RF DNA and ssDNA, respectively. (d and e) The RTLs of the *fpsA* and *fpsB* genes, respectively. The transcription levels of pSW2 *fpsA* and *fpsB* in LEP were set at 1. The error bars show the average values and standard deviations resulting from three replicates. Representative results from two independent experiments are shown. The data were analyzed by Student's *t* test. $^{**}P < 0.01$; $^{*}P < 0.05$; ns, not significantly different.

FpsR binds to multiple sites in the *fpsA* promoter and *fpsA–fpsR* intergenic region

A previous study indicated that FpsR binds to the *fpsA* promoter but not to the *fpsR* promoter [13]. In an effort to more precisely characterize the binding sites of FpsR in the *fpsA* promoter and the neighboring region, we used a DNase I footprinting assay to identify the FpsR binding sites. DNA fragments covering the promoter regions of *fpsA* and the intergenic region between *fpsA* and *fpsR* were end-labeled with 6-carboxyfluorescein (FAM), mixed with FpsR protein and then subjected to DNase I digestion. After that, four protected regions were identified by comparing the sequence patterns in the absence or presence of FpsR (Fig. 4a). Further detailed characterization revealed that FpsR binds to four ~25-bp fragments that are upstream of the *fpsA* coding sequence. Surprisingly, only one of these fragments (*O4*) is located in the promoter region of *fpsA*, and the *O3* operator covers the transcriptional start site of *fpsA* (Fig. 4b). Notably, two operator sites (*O1* and *O2*) are located in the intergenic region between *fpsA* and *fpsR* (Fig. 4b). Moreover, we identified a 25-bp binding motif ($T/GN_3TN_3T/GN_3TT/GN_6TTG/AN_2$) based on the sequence of the four operator sites in the *fpsA* promoter and the *fpsA–fpsR* intergenic region (Fig. 4c).

To confirm whether the identified operators are functional in the FpsR regulatory system, point mutations were introduced in the consensus bases of the four FpsR operators to construct four pSW2-derived vectors (pSW2M*O1*, pSW2M*O2*, pSW2M*O3*, pSW2M*O4*) (Fig. 5a). Compared to the pSW2 vector, the base substitution of the four conserved "T"s to "G"s in *O1*, *O2*, and *O4* led to a significant increase in the RTL of *fpsA* and *fpsR*-3′UTR, which are expressed from the two indicated divergent promoters (Fig. 5b and c). Notably, the RTLs of *fpsA* and *fpsR*-3′UTR were significantly decreased in pSW2M*O3* compared with those in pSW2, suggesting that the initiation of transcription was affected by the base substitution because of the location of *O3* (Fig. 4b). Together,

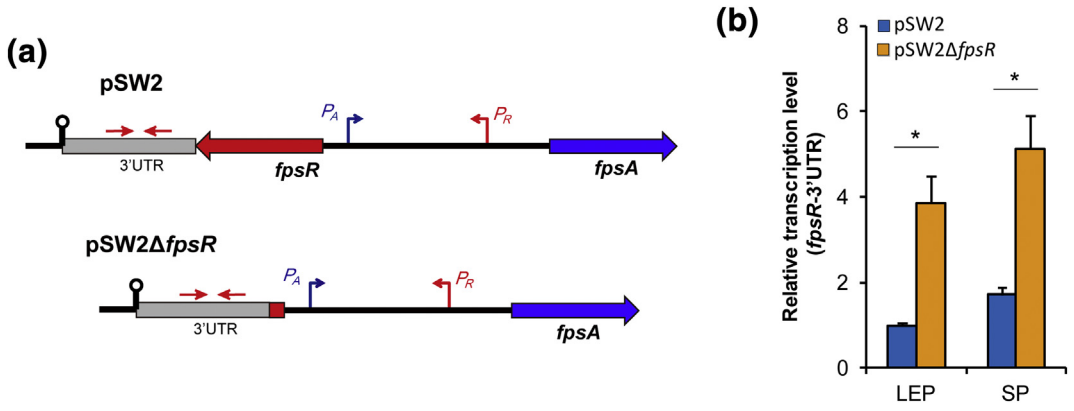

Fig. 3. The transcription of *fpsR* was self-repressed by FpsR. (a) Schematic representation of the operon structure of the wild-type (pSW2) and *fpsR* deletion (pSW2Δ*fpsR*) vectors. The transcription start sites are indicated with angled arrows. The 3′UTR of *fpsR* is shown in gray, and the primer pair used for qPCR is indicated with opposing red arrows. (b) The RTLs of the 3′UTR of the *fpsR* gene. LEP: late exponential phase; SP: stationary phase. The transcription level of *fpsR*-3′UTR in pSW2 in LEP was set at 1. The error bars show the average values and standard deviations resulting from three replicates. Representative results from two independent experiments are shown. The data were analyzed by Student's *t* test. $^*P < 0.05$.

these data indicated that these operators truly play a role in the FpsR regulatory circuit.

The binding affinity of FpsR to operator *O2* and *O3* is higher at low temperature

To examine the binding affinity of FpsR for its four different operators, a real-time surface plasmon resonance (SPR) technique was used to analyze the direct interaction between FpsR and the four operator sites at different temperatures. Biotin-labeled operators *O1–O4* were immobilized on streptavidin biosensor probes. Binding of FpsR to immobilized operators was demonstrated by a series of sensorgrams, which showed the SPR response units (RU) as a function of time (Fig. 6). These changes were fitted to a one-site binding model, thus allowing the association (K_a) and dissociation (K_d) rate constants for DNA binding by FpsR to be calculated. The parameters of the protein–DNA interaction are presented in Table 1. FpsR was able to interact directly with all operators with a dissociation constant in the nanomolar range (7.2–26.2 nM) at 20 °C. The four operators were all associated with similar equilibrium dissociation constants (K_D) of between 8.6 and 10.9 nM at 4 °C. Notably, the SPR assays demonstrated that the K_D value of FpsR-*O2* and FpsR-*O3* at 4 °C (10.4 nM and 8.6 nM) was approximately 2- and 3-fold lower, respectively, than that at 20 °C (Table 1), indicating that the binding affinity of FpsR to these operators is increased at low temperature. However, we also noticed that the K_D value of FpsR-*O4* at 4 °C (10.9 nM) was 1.5-fold-higher than that at 20 °C (7.2 nM). Therefore, at present it is not entirely certain whether the transcription-repression activity of FpsR is higher at low temperature.

Solution multimeric state of FpsR and mutational analysis of its C-terminal region

The N-terminal region of FpsR contains a helix-turn-helix DNA-binding element similar to that of the CTXΦ phage repressor RstR, whereas the C-terminal region is unrelated to the oligomerization domain of the RstR repressor (Fig. S3). However, according to the prediction of the secondary structure by the PSIPRED method [39], two α helices may be formed (Fig. 7a), and these α helices may play a role in the formation of FpsR polymers. After affinity purification, the oligomeric state of FpsR in solution was first probed by size-exclusion chromatography. As shown in Fig. 7b, FpsR eluted as a single peak and, when compared with protein markers, has an apparent molecular mass of 65 kDa. The monomeric mass of FpsR is 16 kDa; thus, we suggest that the major peak represents the tetramers of FpsR. As no other peaks were observed, these data indicate that the FpsR monomer spontaneously formed tetramers in the elution buffer. To investigate the function of C-terminal of FpsR, a 135-bp fragment that encodes the C-terminal region of FpsR was deleted, and the vector pSW2*fpsR*ΔC was constructed. The RTLs of *fpsA* and *fpsR*-3′UTR were significantly increased in pSW2*fpsR*ΔC (see Fig. S4). Furthermore, point mutations were introduced into the C-terminal region of FpsR, and two vectors, pSW2*fpsR*PM1 and pSW2*fpsR*PM2, which harbor the K89P/E90P and N107P/G108P amino acid substitutions, respectively, were constructed (Fig. 7a). The replacements with proline residues were expected to reduce the conformational degrees of freedom in the main polypeptide [40], thus disrupting the structure and function of FpsR protein. Although only the oligomeric state of FpsRPM2 was significantly

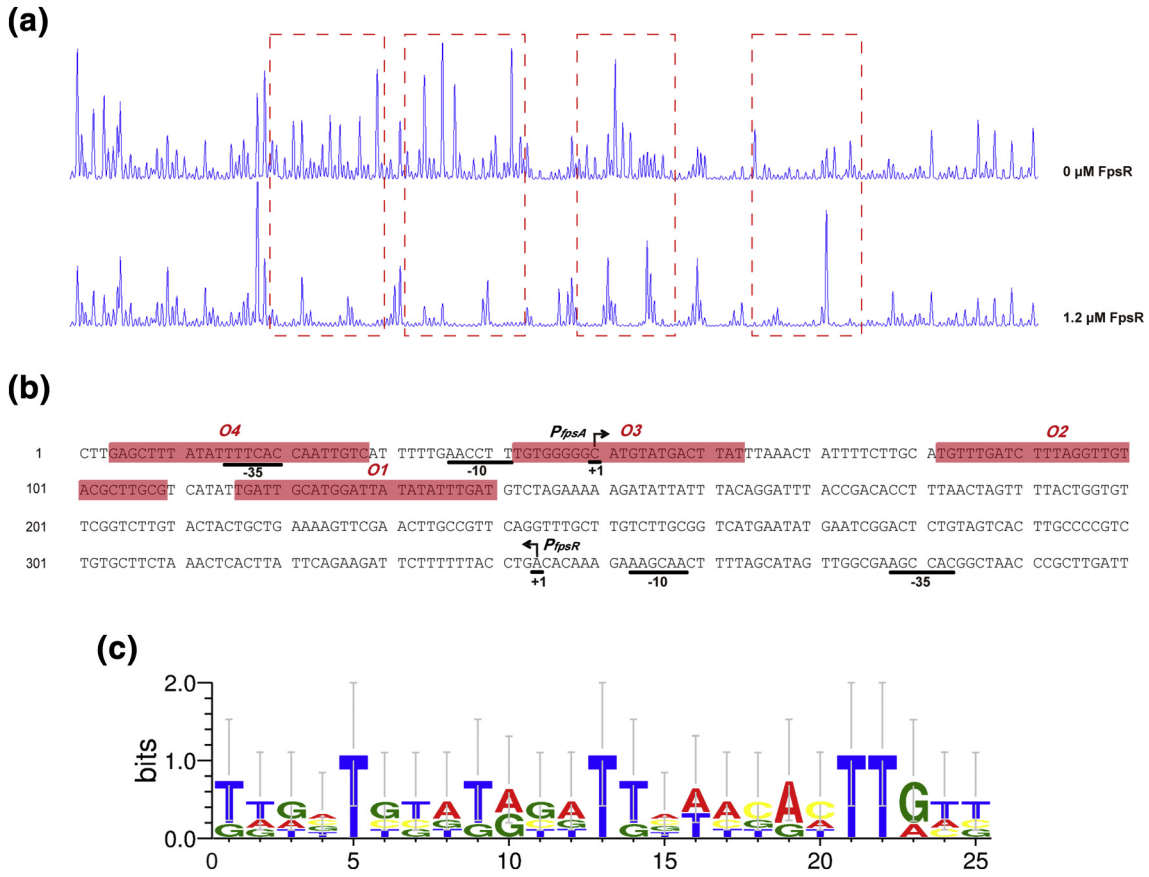

Fig. 4. Identification of the FpsR operator sites in the *fpsA* promoter and the *fpsA–fpsR* intergenic region. (a) Determination of the sequence of the FpsR-protected regions by DNase I protection footprinting. A concentration of 0.05 μM probe covering the entire intergenic region of *fpsA* and *fpsR* was incubated with FpsR (1.2 μM) in EMSA buffer. The DNA fragments were labeled with FAM dye. The regions protected by FpsR from DNase I cleavage are indicated with red dotted boxes. (b) Sequences of the intergenic regions containing operators. The transcription start sites of the *fpsA* and *fpsR* genes are underlined and marked with angled arrows. The −35/−10 consensus elements of *fpsA* and *fpsR* are underlined with solid lines. The operator sites (*O1–O4*) are highlighted in red. (c) The identification of the FpsR binding motif. The sequence logo of the position-specific weight matrix generated by the WebLogo sequence generator program is presented [38]. The error bars indicate the SD of the sequence conservation.

changed as shown by size-exclusion chromatography analysis (Fig. 7b), the subsequent qPCR analysis showed that the RTLs of *fpsA* and *fpsR*-3′UTR were significantly increased in both vectors (Fig. 7c and d). Furthermore, the SPR assay demonstrated that the binding affinities of FpsRPM1 and FpsRPM2 to *O1–O4* were all decreased at 20 °C (Fig. S5 and Table S2). These results indicated that one of the α helices in FpsR C-terminal is responsible for the oligomerization, and both of them affect the DNA-binding activity of FpsR protein, thus significantly influencing the regulatory function of FpsR.

Discussion

Based on the results above, FpsR was demonstrated to be a crucial repressor that controls SW1 transcription. A series of FpsR operator sites were identified in the *fpsA* promoter and the *fpsA–fpsR* intergenic region. In view of these findings, we speculated that RNA polymerases originating at the *fpsR* promoter region will encounter the FpsR-operator complex and that this interference will thereby inhibit transcription. Therefore, more leader transcripts than downstream transcripts should be generated. To confirm this speculation, we quantified different transcripts originating at the *fpsR* promoter (Fig. S6a). The total RNA of WP3ΔSW1–pSW2 was reverse-transcribed, and the Ct values of *fpsAR*-5′UTR (leading transcript) and *fpsR* (downstream transcript) were detected by real-time qPCR using cDNA. The lower Ct value for *fpsAR*-5′ UTR indicates a higher transcript number for *fpsAR*-5′ UTR than for *fpsR* (Fig. S6b and S6c). Taken together, the binding of FpsR to its cognate operators modulated the transcription of P_A and P_R by inhibiting the process of RNA polymerase-mediated transcription. Notably,

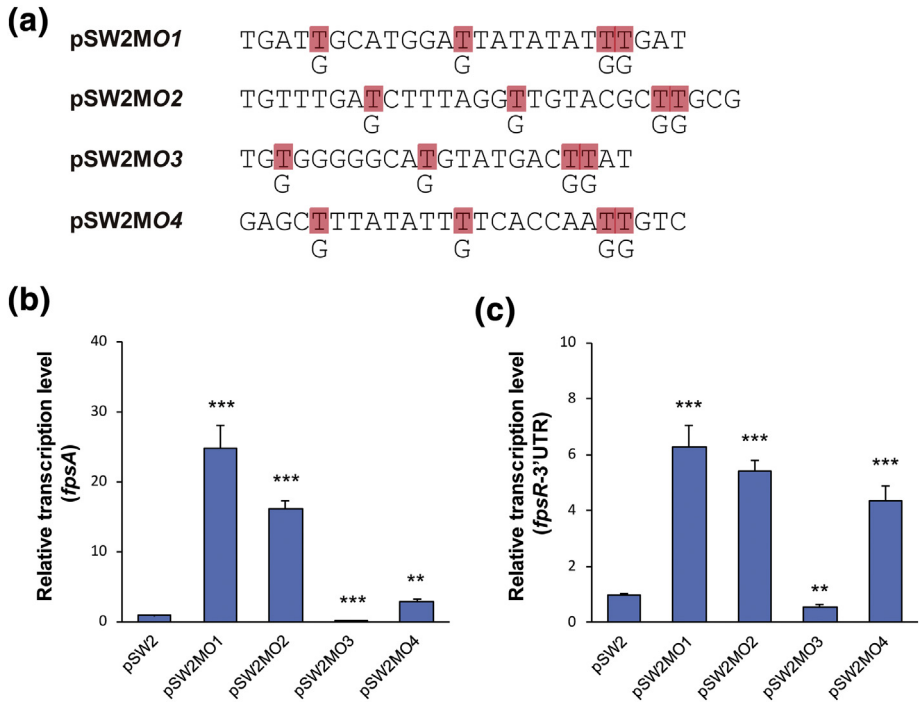

Fig. 5. Functional analysis of the FpsR operators. (a) Construction of four pSW2-derived vectors in which the consensus "T" within the FpsR operators (*O1–O4*) was replaced with "G". The substituted bases are highlighted in red. (b and c) The RTLs of *fpsA* and *fpsR*-3′UTR in pSW2-derived vectors, respectively. The transcription levels of *fpsA* and *fpsR*-3′UTR in pSW2 were set at 1. The error bars show the average values and standard deviations resulting from three replicates. Representative results from three independent experiments are shown. The data were analyzed by Student's *t* test. ***$P < 0.001$; **$P < 0.01$.

both of the steric hindrance and "Roadblock" mechanisms are involved in the transcriptional repression process (Fig. 8).

Repressor-mediated regulation is critical to the life strategy (lysogenic or lytic growth) decision of temperate phages. The repressor RstR of the filamentous phage CTXΦ has been extensively investigated [31,32,41]. RstR has been shown to bind to three operator sites in the *rstA* promoter region. Moreover, the binding of RstR to the *rstR* promoter of results in self-feedback inhibition of gene expression [31]. Although the SW1-encoded repressor FpsR shares some similarities with the RstR repressor, it has a number of distinct features (Fig. 8). RstR has been shown to oligomerize to form dimers and tetramers and to become tetrameric when bound to operator DNA [31], but only tetramers of FpsR were detected by the gel permeation assay (Fig. 7). Furthermore, RstR possesses three operator sites in the *rstA–rstR* intergenic region, whereas four FpsR operators located in the *fpsA–fpsR* intergenic region were identified (Fig. 4). Interestingly, notwithstanding that FpsR cannot bind to the *fpsR* promoter, FpsR is able to participate in autoregulation (Fig. 3). The four identified FpsR operators are located downstream of P_R. In addition, we noticed that one of the three RstR operator sites is also located downstream of the *rstR* promoter [31,42], suggesting that this mechanism may also play a role in the self-repression of RstR.

In λ phage, temperature has previously been found to affect the lysis-lysogeny mechanism of and phage DNA replication, which was completely blocked at low temperature (20 °C) [43,44]. Moreover, phage Bp-AMP1, which was isolated from the tropical pathogen *Burkholderia pseudomallei*, was demonstrated to follow a lytic or temperate lifestyle according to temperature: Bp-AMP1 enters the lytic cycle at 37 °C and remains temperate at 25 °C [45]. Nevertheless, no further investigation has been performed, and it is not clear how these putative thermoregulated genetic switches function. In the present study, we demonstrate that the binding affinity of FpsR to operator sites is different at 20 °C and 4 °C (Table 1), thus contributing to explain the cold induction of phage SW1. Intriguingly, FpsR still controlled the production level of SW1 at 4 °C when the synthesis of phage particles was active [9,12]. We hypothesized that this function is important because it can prevent excessive phage generation, which may influence the host bacterial survival in the cold benthic environments.

The repressors identified in filamentous phage genomes have been demonstrated to have almost no homology at the nucleotide and amino acid

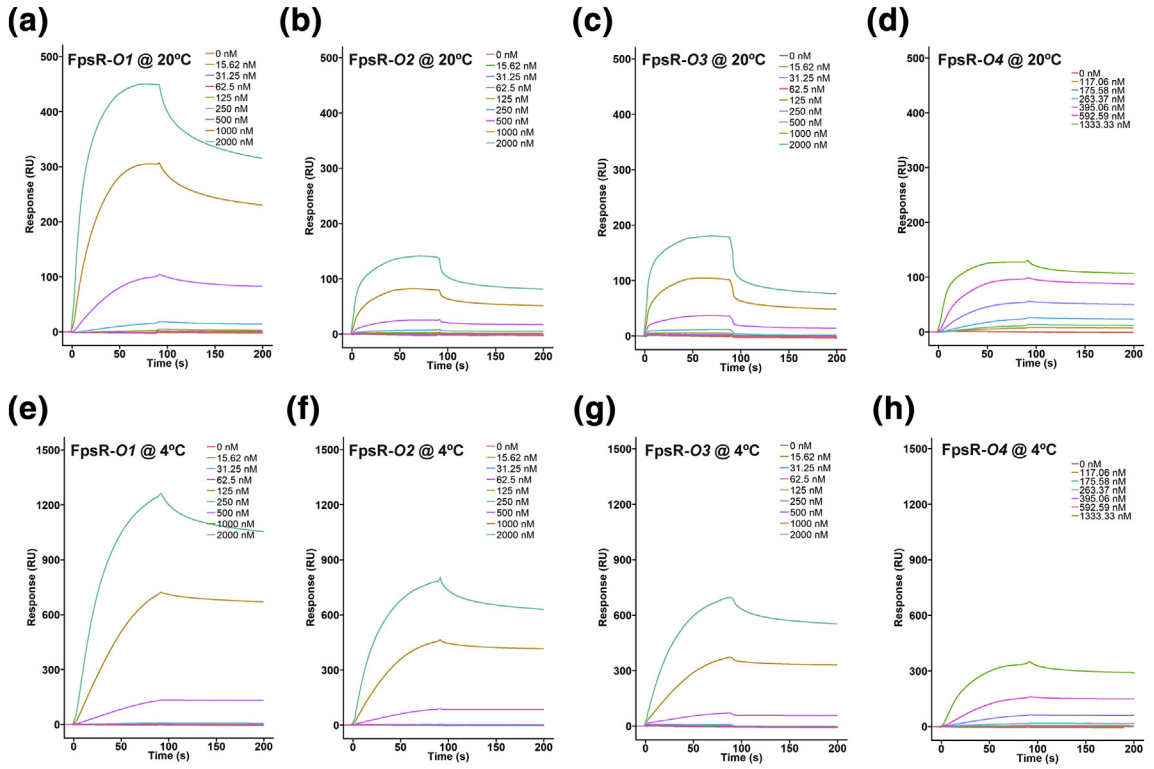

Fig. 6. SPR sensorgrams of the binding of FpsR with the four operator sites (*O1–O4*) at 20 °C (a–d) and 4 °C (e–h), respectively. The FpsR protein was injected over the sensor chip at concentrations ranging from 0 to 2000 nM, and the DNA-binding activity is given in response units (RU).

levels [30]. For example, the highest similarity was observed between the *Xanthomonas* Cf1 and the *Ralstonia* RSM phage repressors, but the similarity is less than 20% (amino acid similarity) [30,46]. In accordance with this finding, the similarity between FpsR and other filamentous phage repressors is very low (6%–27% amino acid identity). This phenomenon encouraged us to speculate that the *Inovirus* repressors may originate from divergent sources. Although two sets of inverted repeats of the form CTNN(A/C)AAG were found in the *O1* operator, such repeats were absent in *O2* and *O3* of RstR, suggesting that consensus binding sites for this type of regulatory factor were difficult to identify [31]. In this study, we identified a 25-bp binding motif with several conserved bases in the four operator sites of FpsR (Fig. 4c). A search of the WP3 genome with this consensus sequence revealed 1666 putative FpsR binding sites, of which 339 sites are located in intergenic regions (data not shown). Furthermore, our previous study indicated that SW1 had a significant impact on the transcription of genes responsible for basic cellular activities, including the transcriptional/translational apparatus, arginine synthesis, purine metabolism, and the flagellar motor [47]. In addition, the lateral flagellar system of WP3 was shown to be influenced by the SW1 phage at low temperatures [37]. It would be interesting to verify whether FpsR regulates these genes of the host bacterium in future investigations. It is worth noting that although the phage-encoded repressors and the cognate operator DNA have been extensively studied in several model phages such as λ, TP901-1, Φ11, and 933 W [15–22,24–27,48–50], the investigation of the regulators of bacteriophage from extreme deep-sea environments provides new insights into the molecular mechanism of genetic switch.

Materials and Methods

Bacterial strains, culture conditions, and growth assay

All bacterial strains and plasmids used in this study are listed in Table 2. The *Shewanella* strains were cultured in modified 2216E marine medium (2216E) (5 g/l tryptone, 1 g/l yeast extract, 0.1 g/l $FePO_4$, and 34 g/l NaCl) with shaking at 220 rpm at different temperatures. The *E. coli* strain WM3064 was incubated in lysogeny broth (LB) medium (10 g/l tryptone, 5 g/l yeast extract, and 10 g/l NaCl) supplemented with 50 μg/ml DL-α, ε-diaminopimelic acid (DAP) at 37 °C. For the solid medium, agar-A (Bio Basic Inc., Ontario, Canada) was added at 1.5% (w/v). The antibiotic chloramphenicol (Cm) (Sigma, St. Louis,

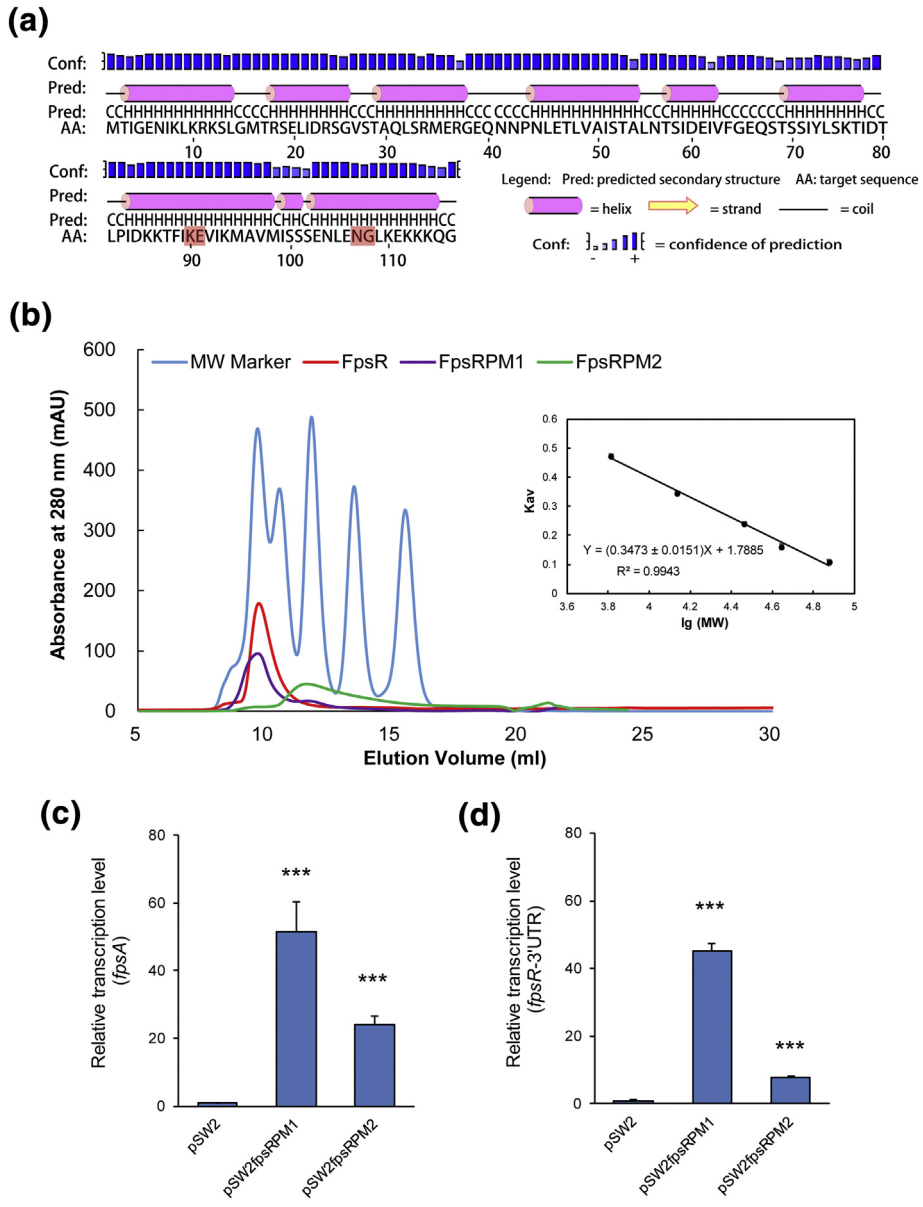

Fig. 7. Determination of the oligomeric state of FpsR and mutational analysis of its C-terminal region. (a) Prediction of the FpsR protein secondary structure. The elements of the secondary structure are represented by helix, strand, and coil designators. The prediction is based on the results from the secondary structure prediction program (the PSIPRED server). The substituted amino acids in the C-terminal region of FpsR are highlighted in red. (b) Gel permeation chromatography of FpsR and its mutants. Size-exclusion chromatograms for FpsR (red), FpsRPM1 (purple), FpsRPM2 (green), and the molecular weight markers (blue; 75, 43, 29, 13.7, and 6.5 kDa) are overlaid. The inset graph shows a standard plot for the molecular masses of the protein standards against the ratio of their elution volumes (*Ve*) and void volumes (*Vo*) (black diamonds). The K_{av} value observed for FpsR corresponds to a molecular mass of ~65 kDa. (c and d) The RTLs of *fpsA* and *fpsR*-3′UTR in pSW2-derived vectors with point mutations in the C-terminal region of FpsR. The transcription levels of *fpsA* and *fpsR*-3′UTR in pSW2 were set at 1. The error bars show the average values and standard deviations resulting from three replicates. Representative results from three independent experiments are shown. The data were analyzed by Student's *t* test. ***$P < 0.001$.

MO, USA) was added to the medium at 25 and 12.5 μg/ml for *E. coli* and *Shewanella* strains, respectively, when required. The growth of the WP3 strains was determined using turbidity measurements at 600 nm in 2216E.

Construction of vectors with *fpsR* and operator mutations

Construction of the vectors harboring the *fpsR* deletion was performed using the *E. coli-Shewanella*

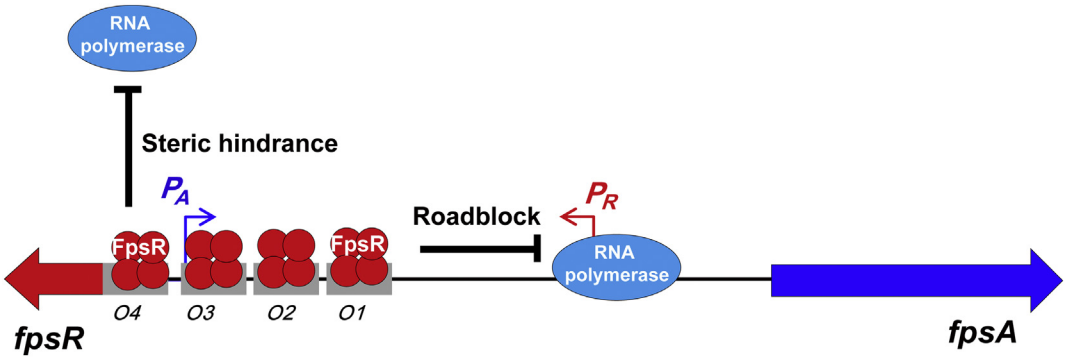

Fig. 8. Schematic model of FpsR involvement in the genetic switch of phage SW1. FpsR binds to four operators that are located in the *fpsA* promoter and in the intergenic region between *fpsA* and *fpsR*. The transcriptions of P_A and P_R by RNA polymerase were inhibited due to the steric hindrance and "Roadblock" mechanisms. The genes and regulatory elements are not drawn to scale.

shuttle vector pSW2, which was constructed based on the replicative form of SW1 and which contained the complete sequence of *fpsR–fpsD* (see Fig. S1 in the supplemental material). Briefly, two opposing primers located in the *fpsR* gene of SW1 were used to amplify the whole sequence of pSW2 except for the coding region of *fpsR*. The PCR products were digested with *Apa* I and then self-ligated, yielding pSW2Δ*fpsR*. The vector pSW2*fpsR*ΔC was constructed by the same strategy. For the construction of vectors with point mutations in the FpsR C-terminal region, primers with different base substitutions were used to amplify the *fpsR* gene. The PCR products were ligated with the remaining pSW2 fragment, yielding pSW2*fpsR*PM1 and pSW2*fpsR*PM2. The same strategy was used to construct the vectors pSW2M*O1*, pSW2M*O2*, pSW2M*O3*, and pSW2M*O4*. The pSW2 vector and its derived vectors were transformed into WM3064, which is a DAP auxotroph strain. The transformants were confirmed by enzyme digestion and DNA sequencing. The vectors were introduced into WP3ΔSW1 by two-parent conjugation. The transconjugant was selected by chloramphenicol resistance and was verified by PCR and enzyme digestion.

Construction of expression plasmids

The expression plasmids pET24b-*fpsR*PM1 and pET24b-*fpsR*PM2 were constructed using the expression vector pET-24b (Novagen, Madison, WI, USA). The coding region of the *fpsR* gene was PCR amplified from pSW2*fpsR*PM1 and pSW2*fpsR*PM2, respectively, with *pfu* DNA polymerase using the primer pair FpsR-ex-For/Rev. The PCR product was gel purified and then ligated into the pET-24b vector at the BamHI and HindIII sites. *E. coli* C41(DE3) cells were transformed with this recombinant plasmid and selected on LB medium containing kanamycin. The positive clones were confirmed by enzyme digestion and DNA sequencing.

RNA isolation and real-time qPCR

The WP3 strains were inoculated into 2216E at different temperatures as indicated in the text, and the cultures were collected when the cells reached exponential and stationary phases and were immediately placed in liquid nitrogen. Total RNA extraction, reverse transcription, and real-time qPCR were performed as described previously [11,12,52]. The primer pairs used to amplify the selected genes in the qPCR assay were designed using Primer Express software (Applied Biosystems, Foster City, CA, USA).

DNA copy number determination

The copy number of pSW2 RF DNA and ssDNA was quantified as previously described [12]. In brief, the primer pair SW1RFRTFor/SW1RFRTRev (Table S1) was designed to quantify the copy number of RF DNA because this primer pair is located in the *attP* site of SW1, which uses the RF DNA as the specific amplification template. The total DNA was used as a template for the first round of qPCR; the copy number equaled with RF DNA count plus the ssDNA count. The template for the second round of qPCR was total DNA treated with S1 nuclease (Thermo Fisher Scientific, MA, Waltham, USA). After the ssDNA was removed from the total DNA, the quantification result was the copy number of RF DNA. Finally, the copy number of the ssDNA was calculated from the two rounds of qPCR.

Enumeration of VLPs

To enumerate the VLPs, approximately 2 ml of bacterial culture was centrifuged at 10,000*g* for 1 min. After centrifugation, the supernatant was filtered with a 0.02-μm pore-size Anodisc Al_2O_3 filter (Whatman, Kent, UK), and the filter were stained with 25× SYBR Green I (Invitrogen, Carlsbad, CA, USA) for 15 min in

Table 1. Kinetic parameters for the interaction between FpsR and operators *O1–O4*[a]

DNA	Temperature (°C)	K_D (M)	K_a (1/ms)	K_a error	K_d (1/s)	K_d error
O1	20	1.10E−08	1.02E+05	4.00E+02	1.12E−03	8.40E−06
	4	1.09E−08	4.43E+04	1.10E+02	4.82E−04	2.00E−06
O2	20	1.83E−08	3.62E+04	5.50E+01	6.66E−04	2.70E−06
	4	1.04E−08	4.36E+04	1.28E+02	4.55E−04	2.20E−06
O3	20	2.62E−08	3.50E+04	6.50E+01	9.19E−04	4.20E−06
	4	8.56E−09	4.62E+04	1.30E+02	3.96E−04	2.00E−06
O4	20	7.18E−09	5.56E+04	1.08E+02	3.99E−04	4.20E−06
	4	1.09E−08	2.33E+04	1.80E+01	2.53E−04	1.20E−06

[a] Equilibrium dissociation constants (K_D) were determined by SPR using a Biacore T200 system (GE Healthcare). Errors listed in this table are the standard errors for the fit to a Langmuir 1:1 binding model. K_a, association rate constant; K_d, dissociation rate constant.

the dark. After rinsing with 0.02-μm filter-autoclaved MilliQ H_2O, each filter was mounted on a glass slide with 0.1% (v/v) *p*-phenylenediamine dihydrochloride anti-fade mounting medium (Sangon Biotech, Shanghai, China). VLPs on the filter were observed with a fluorescence microscope (Nikon Eclipse 90i, Melville, NY, USA). For each sample, the number of VLPs was counted in at least 10 microscopic fields, with a total number above 200.

Expression and purification of FpsR proteins

The expression and purification of His-tagged FpsR were performed as previously described [13].

Table 2. Bacterial strains, plasmids, and oligonucleotides used in this study

Strain/Plasmid/Oligonucleotides	Relevant genotype	Reference or source
E. coli strain		
WM3064	Donor strain for conjugation; Δ*dapA*	[51]
C41(DE3)	Recombinant protein expression host	GE Healthcare
S. piezotolerans WP3 strains		
WP3ΔSW1	*S. piezotolerans* WP3 wild-type strain without phage SW1	[37]
WP3ΔSW1–pSW2	WP3△SW1 strain harboring pSW2	This work
WP3ΔSW1–pSW2Δ*fpsR*	WP3△SW1 strain harboring pSW2Δ*fpsR*	This work
WP3ΔSW1–pSW2*fpsR*ΔC	WP3△SW1 strain harboring pSW2-*fpsR*ΔC	This work
WP3ΔSW1–pSW2*fpsR*PM1	WP3△SW1 strain harboring pSW2-*fpsR*M1	This work
WP3ΔSW1–pSW2*fpsR*PM2	WP3△SW1 strain harboring pSW2-*fpsR*M2	This work
WP3ΔSW1–pSW2M*O1*	WP3△SW1 strain harboring pSW2M*O1*	This work
WP3ΔSW1–pSW2M*O2*	WP3△SW1 strain harboring pSW2M*O2*	This work
WP3ΔSW1–pSW2M*O3*	WP3△SW1 strain harboring pSW2M*O3*	This work
WP3ΔSW1–pSW2M*O4*	WP3△SW1 strain harboring pSW2M*O4*	This work
Plasmids		
pSW2	Chl^r, derived from the filamentous bacteriophage SW1	[36]
pSW3	pSW2 containing *pepN*, used for SW1 RF- and ssDNA quantification	[12]
pET24b	Kan^r, His-tag protein expression vector	Novagen
pSW2Δ*fpsR*	pSW2 with deletion of the coding region of *fpsR* gene	This work
pSW2*fpsR*ΔC	pSW2 with deletion of C-terminal domain of *fpsR* gene	This work
pSW2*fpsR*PM1	pSW2 with point mutation of FpsR at positions 89 (K to P) and 90 (E to P)	This work
pSW2*fpsR*PM2	pSW2 with point mutation of FpsR at positions 107 (N to P) and 108 (G to P)	This work
pSW2M*O1*	pSW2 with point mutation of FpsR operator *O1*	This work
pSW2M*O2*	pSW2 with point mutation of FpsR operator *O2*	This work
pSW2M*O3*	pSW2 with point mutation of FpsR operator *O3*	This work
pSW2M*O4*	pSW2 with point mutation of FpsR operator *O4*	This work
pET24b-*fpsR*	pET24b containing the coding region of the *fpsR* gene	[13]
pET24b-*fpsR*PM1	pET24b containing the coding region of the *fpsR*PM1 gene	This work
pET24b-*fpsR*PM2	pET24b containing the coding region of the *fpsR*PM2 gene	This work
Oligonucleotides		
O1	5′-Biotin-TCTAGACATCAAATATATAATCCAT GCAATCAATATGACGCAAGCGTACA-3′ (50 bp)	This work
O2	5′-Biotin-CAATATGACGCAAGCGTACAACCTA AAGATCAAACATGCAAGAAAATAGT-3′ (50 bp)	This work
O3	5′-Biotin-AGAAAATAGTTTAAATAAGTCATAC ATGCCCCCACAAAGGTTCAAAAATG-3′ (50 bp)	This work
O4	5′-Biotin-TTTTACGCTTGAGCTTTATATTTTCA CCAATTGTCATTTTTGAACCTTTG-3′ (50 bp)	This work

Briefly, the *E. coli* strain C41 (DE3), which contains the FpsR expression vector, was grown in 1 l of LB broth with 50 μg/ml kanamycin at 37 °C for 3 h. FpsR expression was induced by the addition of 0.5 mM IPTG when the OD_{600} reached 1.0, and the culture was then incubated at 20 °C overnight. The cells were collected by centrifugation, resuspended in binding buffer [500 mM NaCl, 20 mM imidazole, and 20 mM Tris–HCl (pH 8.0)] and sonicated on ice. The cell extract was clarified by centrifugation at 10,000*g* for 20 min at 4 °C. Ni Sepharose High Performance (GE Healthcare, Milwaukee, WI, USA) resin was used to purify the His-tagged FpsR according to the manufacturer's instructions. The protein was eluted in elution buffer [500 mM NaCl, 500 mM imidazole, and 20 mM Tris–HCl (pH 8.0)]. Imidazole was removed using HiTrap desalting columns (GE Healthcare) according to the manufacturer's instructions. The same procedure was used for expression and purification of FpsRPM1 and FpsRPM2. The purified proteins were stored at 4 °C, and its concentration was determined by the Bradford method using bovine serum albumin as a standard. The purity of proteins was confirmed by SDS-PAGE (15% acrylamide) with visualization using Coomassie Brilliant Blue R-250.

Size-exclusion chromatography

Purified FpsR proteins were dialyzed into PBS buffer and run over a Superdex 75,100/300 GL column (GE Healthcare) at 20 °C. The elution fractions were collected, and peaks were identified with UV absorbance measurements at 280 nm. The gel filtration molecular weight markers (GE Healthcare) were resuspended in the same buffer at the manufacturer-recommended concentrations and run over the same column. Specific proteins used for the standard curve included aprotinin (6.5 kDa), ribonuclease (13.7 kDa), carbonic anhydrase (29.0 kDa), ovalbumin (43 kDa), and conalbumin (75 kDa). The molecular masses of the gel filtration standards were plotted against elution volume (Ve) over void volume (Vo) to determine the molecular mass of FpsR proteins based on its elution volume.

DNase I footprinting

For preparation of the probe, the intergenic region of SW1 was PCR-amplified with a 5′ FAM-labeled primer (Table S1) using plasmid pSW2 as the template. The FAM-labeled probe was purified with a gel extraction kit (Tiangen Biotech, Beijing, China) and quantified with a NanoDrop 2000C spectrophotometer (Thermo Fisher Scientific). For each assay, 1 pmol probe was incubated with 24 pmol FpsR in a total volume of 20 μl in the binding buffer [40 mM KCl, 125 μM $MnCl_2$, 1.25 mM $MgCl_2$, 5% glycerol (v/v), 0.5 mM DTT, 5 μg/ml bovine serum albumin, and 5 ng/μl poly(-dIdC), and 12.5 mM Tris (pH 7.5)]. After incubation for 30 min at 20 °C, 10 μl of solution containing 0.015 U of DNase I (Takara Bio Inc., Kyoto, Japan) was added, and the mixture was further incubated for 1 min at room temperature. The reaction was stopped by adding stop solution containing 200 mM unbuffered sodium acetate, 30 mM EDTA and 0.15% SDS (w/v). The digested samples were first extracted with phenol/chloroform and then precipitated with ethanol, and the pellets were dissolved in 20 μl Mini-Q water. The digested fragments were separated by capillary electrophoresis, and the peak heights on the chromatograms were determined. The protocols for DNA ladder preparation, gel electrophoresis, and data analysis were the same as described previously, except that the ROX500 size standard (Applied Biosystems) was used.

SPR measurements

Biacore T200 instruments (GE Healthcare) were used to evaluate the binding affinity of FpsR and its mutants to *O1–O4* DNA via SPR. Briefly, 10 nmol/l of biotinylated operator DNA was captured on the surface of SA chip at a flow rate of 30 μl/min for 90 s in phosphate-buffered saline with 0.05% (v/v) Tween-20 at pH 7.4. Series concentrations of FpsR proteins were injected into the flow system and analyzed, respectively. All binding analysis was performed in phosphate-buffered saline with 0.05% (v/v) Tween-20 (pH 7.4) at both 4 °C and 20 °C. The association time was set to 90 s, while the dissociation time was set to 360 s. After dissociation, the chip surface was regenerated by 10 mM NaOH for 15 s and stabilized for 120 s. Prior to analysis, double-reference subtractions were made to eliminate bulk refractive index changes, injection noise, and data drift. The binding affinity was determined by global fitting to a Langmuir 1:1 binding model within the Biacore Evaluation software (GE Healthcare).

Acknowledgments

This work was financially supported by the National Key R&D Program of China (Grant No. 2018YFC0309800) and the National Natural Science Foundation of China (Grant Nos. 41676118 and 41530967).

Appendix A. Supplementary data

Supplementary data to this article can be found online at https://doi.org/10.1016/j.jmb.2019.01.040.

Received 8 August 2018;
Received in revised form 16 January 2019;
Accepted 31 January 2019
Available online 7 February 2019

Keywords:
filamentous phage;
transcriptional repression;
FpsR;
repressor;
deep sea

†H.H.J., G.P.X., and S.Z.L. contributed equally to this work.

Abbreviations used:
RF DNA, replicative double-stranded DNA; ssDNA, single-stranded DNA; UTRs, untranslated regions; RTL, relative transcription level; VLPs, virus-like particles; FAM, 6-carboxyfluorescein; K_a, association rate constant; K_d, dissociation rate constant; P_A, promoter of *fpsA* gene; P_R, promoter of *fpsR* gene.

References

[1] C.A. Suttle, Marine viruses—major players in the global ecosystem, Nat. Rev. Microbiol. 5 (2007) 801–812.
[2] M. Breitbart, Marine viruses: truth or dare, Annu. Rev. Mar. Sci. 4 (2012) 425–448.
[3] F. Rohwer, R.V. Thurber, Viruses manipulate the marine environment, Nature 459 (2009) 207–212.
[4] C.A. Suttle, Viruses in the sea, Nature 437 (2005) 356–361.
[5] R. Danovaro, A. Dell'Anno, C. Corinaldesi, M. Magagnini, R. Noble, C. Tamburini, et al., Major viral impact on the functioning of benthic deep-sea ecosystems, Nature 454 (2008) 1084–1087.
[6] R. Danovaro, A. Dell'Anno, C. Corinaldesi, Eugenio Rastelli, R. Cavicchioli, M. Krupovic, et al., Virus-mediated archaeal hecatomb in the deep seafloor, Sci. Adv. 2 (2016).
[7] A. Dell'Anno, C. Corinaldesi, R. Danovaro, Virus decomposition provides an important contribution to benthic deep-sea ecosystem functioning, Proc. Natl. Acad. Sci. U. S. A. 112 (2015) E2014–E2019.
[8] R. Danovaro, C. Corinaldesi, G.M. Luna, M. Magagnini, E. Manini, A. Pusceddu, Prokaryote diversity and viral production in deep-sea sediments and seamounts, Deep-Sea Res. II Top. Stud. Oceanogr. 56 (2009) 738–747.
[9] F. Wang, F. Wang, Q. Li, X. Xiao, A novel filamentous phage from the deep-sea bacterium *Shewanella piezotolerans* WP3 is induced at low temperature, J. Bacteriol. 189 (2007) 7151–7153.
[10] X. Xiao, P. Wang, X. Zeng, D.H. Bartlett, F. Wang, *Shewanella psychrophila* sp. nov. and *Shewanella piezotolerans* sp. nov., isolated from West Pacific deep-sea sediment, Int. J. Syst. Evol. Microbiol. 57 (2007) 60–65.
[11] F. Wang, J. Wang, H. Jian, B. Zhang, S. Li, F. Wang, et al., Environmental adaptation: genomic analysis of the piezotolerant and psychrotolerant deep-sea iron reducing bacterium *Shewanella piezotolerans* WP3, PLoS One 3 (2008), e1937.
[12] H. Jian, J. Xu, X. Xiao, F. Wang, Dynamic modulation of DNA replication and gene transcription in deep-sea filamentous phage SW1 in response to changes of host growth and temperature, PLoS One 7 (2012), e41578.
[13] H. Jian, L. Xiong, G. Xu, X. Xiao, F. Wang, Long 5′ untranslated regions regulate the RNA stability of the deep-sea filamentous phage SW1, Sci. Rep. 6 (2016), 21908.
[14] G.F. Hatfull, R.W. Hendrix, Bacteriophages and their genomes, Curr. Opin. Virol. 1 (2011) 298–303.
[15] M. Pedersen, L.L. Leggio, J.G. Grossmann, S. Larsen, K. Hammer, Identification of quaternary structure and functional domains of the CI repressor from bacteriophage TP901-1, J. Mol. Biol. 376 (2008) 983–996.
[16] S. Stayrook, P. Jaru-Ampornpan, J. Ni, A. Hochschild, M. Lewis, Crystal structure of the λ repressor and a model for pairwise cooperative operator binding, Nature 452 (2008) 1022–1025.
[17] M. Pedersen, M. Ligowska, K. Hammer, Characterization of the CI repressor protein encoded by the temperate lactococcal phage TP901-1, J. Bacteriol. 192 (2010) 2102–2110.
[18] A.H. Johansen, L. Brøndsted, K. Hammer, Identification of operator sites of the CI repressor of phage TP901-1: evolutionary link to other phages, Virology 311 (2003) 144–156.
[19] A. Biswas, S. Mandal, S. Sau, Identification and characterization of a CI binding operator at a distant location in the temperate staphylococcal phage Φ11, FEMS Microbiol. Lett. 364 (2017) fnx201.
[20] I.B. Dodd, A.J. Perkins, D. Tsemitsidis, J.B. Egan, Octamerization of λ CI repressor is needed for effective repression of P_{RM} and efficient switching from lysogeny, Genes Dev. 15 (2001) 3013–3022.
[21] K.K. Rasmussen, K.E.H. Frandsen, E.B. Erba, M. Pedersen, A.K. Varming, K. Hammer, et al., Structural and dynamics studies of a truncated variant of CI repressor from bacteriophage TP901-1, Sci. Rep. 6 (2016) 29574.
[22] M. Lewis, A tale of two repressors, J. Mol. Biol. 409 (2011) 14–27.
[23] I.B. Dodd, K.E. Shearwin, J.B. Egan, Revisited gene regulation in bacteriophage λ, Curr. Opin. Genet. Dev. 15 (2005) 145–152.
[24] M. Das, T. Ganguly, P. Chattoraj, P.K. Chanda, A. Bandhu, C.Y. Lee, et al., Purification and characterization of repressor of temperate *Staphylococcus aureus* Φ11, J. Biochem. Mol. Biol. 40 (2007) 740–748.
[25] M. Das, T. Ganguly, A. Bandhu, R. Mondal, P.K. Chanda, B. Jana, et al., Moderately thermostable phage Φ11 Cro repressor has novel DNA binding capacity, BMB Rep. 42 (2008) 160–165.
[26] T. Ganguly, M. Das, A. Bandhu, P.K. Chanda, B. Jana, R. Mondal, et al., Physicochemical properties and distinct DNA binding capacity of the repressor of temperate *Staphylococcus aureus* phage Φ11, FEBS J. 276 (2009) 1975–1985.
[27] A. Biswas, S. Mandal, S. Sau, The N-terminal domain of the repressor of *Staphylococcus aureus* phage Φ11 possesses an unusual dimerization ability and DNA binding affinity, PLoS One 9 (2014), e95012.
[28] J. Rakonjac, N.J. Bennett, J. Spagnuolo, D. Gagic, M. Russel, Filamentous bacteriophage biology, phage display and nanotechnology applications, Curr. Issues Mol. Biol. 13 (2010) 51–76.
[29] J. Rakonjac, Filamentous bacteriophages: biology and applications, eLS, 2012.
[30] A. Mai-Prochnow, J.G.K. Hui, S. Kjelleberg, J. Rakonjac, D. McDougald, S.A. Rice, Big things in small packages: the genetics of filamentous phage and effects on fitness of their host, FEMS Microbiol. Rev. 39 (2015) 465–487.
[31] H.H. Kimsey, M.K. Waldor, The CTXΦ repressor RstR binds DNA cooperatively to form tetrameric repressor–operator complexes, J. Biol. Chem. 279 (2004) 2640–2647.

[32] M.K. Waldor, E.J. Rubin, G.D.N. Pearson, H. Kimsey, J.J. Mekalanos, Regulation replication and integration functions of CTXΦ are encoded by region RS2, Mol. Microbiol. 24 (1997) 917–926.
[33] G.-J. Shieh, Y.-C. Charng, Jenn-Tu Bei-ChangYang, H.-J. Bau, T.-T. Kuo, Identification and nucleotide sequence analysis of an open reading frame involved in high frequency conversion of turbid to clear plaque mutants of filamentous phage Cf1t, Virology 185 (1991) 316–322.
[34] C.-M. Cheng, H.-J. Wang, H.-J. Bau, T.-T. Kuo, The primary immunity determinant in modulating the lysogenic immunity of the filamentous bacteriophage cf, J. Mol. Biol. 287 (1999) 867–876.
[35] H.S. Addy, A. Askora, T. Kawasaki, M. Fujie, T. Yamada, Loss of virulence of the phytopathogen *Ralstonia solanacearum* through infection by ΦRSM filamentous phages, Phytopathology 102 (2012) 469–477.
[36] X. Yang, H. Jian, F. Wang, pSW2, a novel low-temperature-inducible gene expression vector based on a filamentous phage of the deep-sea bacterium *Shewanella piezotolerans* WP3, Appl. Environ. Microbiol. 81 (2015) 5519–5526.
[37] H. Jian, X. Xiao, F. Wang, Role of filamentous phage SW1 in regulating the lateral flagella of *Shewanella piezotolerans* strain WP3 at low temperatures, Appl. Environ. Microbiol. 79 (2013) 7101–7109.
[38] G.E. Crooks, G. Hon, J.-M. Chandonia, S.E. Brenner, WebLogo: a sequence logo generator, Genome Res. 14 (2004) 1188–1190.
[39] D.W.A. Buchan, F. Minneci, T.C.O. Nugent, K. Bryson, D.T. Jones, Scalable web services for the PSIPRED protein analysis workbench, Nucleic Acids Res. 41 (2013) W349–W357.
[40] K. Watanabe, Y. Suzuki, Protein thermostabilization by proline substitutions, J. Mol. Catal. B Enzym. 4 (1998) 167–180.
[41] B.M. Davis, H.H. Kimsey, W. Chang, M.K. Waldor, The *Vibrio cholerae* O139 Calcutta bacteriophage CTXΦ is infectious and encodes a novel repressor, J. Bacteriol. 181 (1999) 6779–6787.
[42] B.E. Nickels, A new twist on a classic paradigm: illumination of a genetic switch in *Vibrio cholerae* phage CTXΦ, J. Bacteriol. 191 (2009) 6779–6781.
[43] M. Obuchowski, Y. Shotland, S. Koby, H. Giladi, M. Gabig, G. Wegrzyn, et al., Stability of CII is a key element in the cold stress response of bacteriophage λ infectioin, J. Bacteriol. 179 (1997) 5987–5991.
[44] M. Gabig, M. Obuchowski, S. Srutkowska, G. Wegrzyn, Regulaton of replication of λ phage and λ plasmid DNAs at low temperature, Mol. Gen. Genet. 258 (1998) 494–502.
[45] J. Shan, S. Korbsrisate, P. Withatanung, N.L. Adler, M.R.J. Clokie, E.E. Galyov, Temperature dependent bacteriophages of a tropical bacterial pathogen, Front. Microbiol. 5 (2014) 599.
[46] T. Kawasaki, S. Nagata, A. Fujiwara, H. Satsuma, M. Fujie, S. Usami, et al., Genomic characterization of the filamentous integrative bacteriophages ΦRSS1 and ΦRSM1, which infect *Ralstonia solanacearum*, J. Bacteriol. 189 (2007) 5792–5802.
[47] H. Jian, L. Xiong, G. Xu, X. Xiao, Filamentous phage SW1 is active and influences the transcriptome of the host at high-pressure and low-temperature, Environ. Microbiol. Rep. 8 (2016) 358–362.
[48] A.P. Koudelka, L.A. Hufnagel, G.B. Koudelka, Purification and characterization of the repressor of the Shiga bacteriophage 933W: DNA binding, gene regulation, and autocleavage, J. Bacteriol. 186 (2004) 7659–7669.
[49] T.J. Bullwinkle, G.B. Koudelka, The lysis-lysogeny decision of bacteriophage 933W: a 933W repressor-mediated long-distance loop has no role in regulating 933W P_{RM} activity, J. Bacteriol. 193 (2011) 3313–3323.
[50] T.J. Bullwinkle, D. Samorodnitsky, R.C. Rosati, G.B. Koudelka, Determinants of bacteriophage 933W repressor DNA binding specificity, PLoS One 7 (2012), e34563.
[51] H. Gao, Z.K. Yang, L. Wu, D.K. Thompson, J. Zhou, Global transcriptome analysis of the cold shock response of *Shewanella oneidensis* MR-1 and mutational analysis of its classical cold shock proteins, J. Bacteriol. 188 (2006) 4560–4569.
[52] H. Jian, G. Xu, Y. Gai, J. Xu, X. Xiao, The histone-like nucleoid structuring protein (H-NS) is a negative regulator of the lateral flagellar system in the deep-sea bacterium *Shewanella piezotolerans* WP3, Appl. Environ. Microbiol. 82 (2016) 2388–2398.